

Development and Usage of a Continuously Differentiable Heavy Duty Diesel Engine Model Equipped with VGT and EGR

2017-01-0611

Published 03/28/2017

Viktor Leek, Kristoffer Ekberg, and Lars Eriksson

Linköping University

CITATION: Leek, V., Ekberg, K., and Eriksson, L., "Development and Usage of a Continuously Differentiable Heavy Duty Diesel Engine Model Equipped with VGT and EGR," SAE Technical Paper 2017-01-0611, 2017, doi:10.4271/2017-01-0611.

Copyright © 2017 SAE International

1. Abstract

Today's need for fuel efficient vehicles, together with increasing engine component complexity, makes optimal control a valuable tool in the process of finding the most fuel efficient control strategies. To efficiently calculate the solution to optimal control problems a gradient based optimization technique is desirable, making continuously differentiable models preferable. Many existing control-oriented Diesel engine models do not fully possess this property, often due to signal saturations or discrete conditions. This paper offers a continuously differentiable, mean value engine model, of a heavy-duty diesel engine equipped with VGT and EGR, suitable for optimal control purposes. The model is developed from an existing, validated, engine model, but adapted to be continuously differentiable and therefore tailored for usage in an optimal control environment. The changes due to the conversion are quantified and presented. Furthermore, it is shown and analyzed how to optimally control the engine in a fuel optimal way under steady-state conditions, and in a time optimal way in a tip-in scenario.

EGR and VGT equipped validated heavy-duty mean value Diesel engine model (MVEM) presented in [2]. The approach taken in this work has been adapted to the fact that NOx emission maps have not been available.

The focus of this paper is on finding the performance boundaries of the MVEM, under steady-state, as well as dynamic, conditions. In particular the paper investigates fuel optimal control under steady-state, and time-optimal tip-ins under dynamic conditions, where the effect of EGR is of particular interest. The information gathered from the optimization is intended to be used as a benchmark for evaluating control strategies, i.e. to answer the question how close to optimal the system behaves, and as inspiration for designing causal control strategies.

For the minimum time tip-ins optimal control was used to find solutions to the problems. The applied optimal control method was so-called local direct collocation. The benefit of this method, compared to traditional methods, such as Pontryagin's maximum principle, is that it effectively handles inequality constraints [3]. The downside is that a continuously differentiable model is preferred by the underlying gradient-based optimization routine, in order to effectively find a solution. The MVEM does to a large degree possess this property, but not fully, and therefore needed slight alterations.

Several authors have studied the optimal control of combustion engines. In [4] a comprehensive study of the subject is presented, including details regarding the underlying numerical calculations. It reports the problem of finding the optimal control of a turbocharged and EGR equipped engine as very difficult. This due to the fact that the system has two dynamic loops, the turbocharger and the EGR system, which causes problems in the optimization. Others have studied the steady-state optimal control of Diesel engines, for instance [5], in which emissions reduction and controllability is of particular focus. In [6] the optimal control of a VGT equipped SI engine is studied. In it, it is clearly seen that the optimal VGT behavior is a trade-off between, pumping work, exhaust manifold pressure, and turbine mass flow. Others have used optimal control for

2. Introduction

Vehicles produced today are subjected to legislations whose purpose is to limit their emissions. Nitrogen oxides (NOx) are formed during the combustion process, especially in Diesel engines. The amount of NOx allowed to escape the vehicle is low and therefore makes aftertreatment systems necessary. To aid the aftertreatment system, an exhaust gas recirculation system (EGR) can be used, in which exhaust gas is lead back into the intake manifold, leading to reduced combustion temperature and with that reduced NOx formation [1]. One way of controlling this process is to equip the engine with a variable geometry turbine (VGT). This way the inlet area of the turbine can be reduced, thereby increasing the exhaust manifold pressure, making it possible to pump exhaust gas into the intake manifold, even at low load conditions.

The purpose of this work is to find control strategies for controlling Diesel engines equipped with VGT and EGR using modeling, simulation, and optimization. The starting point of this work is the

solving complex Diesel engine problems, see for instance [7]. For a general treatment of Diesel engine control, the reader is referred to [8] and [1].

The paper is organized as follows. The alterations made to the MVEM are presented and validated in [Section 3](#), the fuel optimal steady-state control and time optimal tip-ins are presented in [Section 4](#), the results are presented and analyzed in [Section 5](#), and conclusions are presented in [Section 6](#).

Contribution

The contributions of this paper are: An optimal control ready mean value engine model of a heavy duty Diesel engine equipped with VGT and EGR. The time-optimal tip-in control of a heavy-duty Diesel engine when both EGR and VGT are actively controlled. Furthermore, a constraint that ensures the EGR mass flow to only flow in the direction from the exhaust to the intake, without limiting the entire optimization to restricted pressure ratios, is presented.

3. Continuously Differentiable Heavy Duty Diesel Engine Model

In this section the model equations are presented. It is shown that the model presented in [2] to a large degree posses the continuously differentiable property, where it does not new equations are presented, motivated and validated.

The complete engine model consists of several subsystems, which describes the different engine components. The implemented models, and the specific model properties are described. This model is an extension of the previously developed model [2]. The main reason for a model to be continuously differentiable is that it allows for gradient based optimization techniques, enabling the model to be used in an optimal control environment. Some of the submodels implemented in [2] has this property, but a few do not and therefore need to be replaced.

Model States and Control Signals

The complete engine model consists of five states ([equation \(1\)](#)) and three control signals ([equation \(2\)](#)). The engine speed (N_{ice}) is treated as a exogenous input into the system.

$$x = [p_{im} \ p_{em} \ X_{oim} \ X_{oem} \ N_{tc}]^T \quad (1)$$

$$u = [u_\delta \ u_{EGR} \ u_{VGT}]^T \quad (2)$$

Cylinder Torque

The engine torque is dependent on the amount of fuel injected in the cylinders, where the burnt fuel generates a torque on the engine crank shaft. The engine losses are divided into the two categories, pumping losses and friction losses. The governing equation describing the delivered torque from the engine (M_{ice}) is described by

$$M_{ice} = M_{ign} - M_{pump} - M_{fr} \quad (3)$$

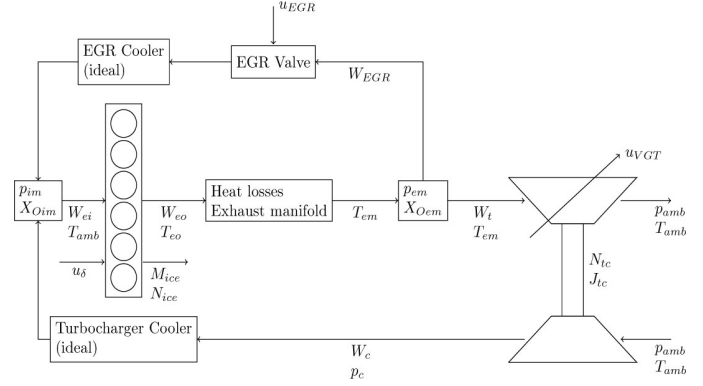


[Figure 1. System drawing, the control signals and the most interesting signals between the different subsystems are viewed.](#)

where M_{ign} is the gross indicated torque generated by the burning the fuel, M_{pump} is the pumping losses calculated as the pressure difference over the cylinders, M_{fr} is the friction torque present inside the crank shaft bearings and the in-cylinder friction. The three torque components are further described by

$$M_{ign} = \eta_{ignch} \left(1 - \frac{1}{r_c^{\gamma_{cyl}-1}} \right) \frac{n_{cyl} q_{HV} u_\delta 10^{-6}}{2\pi n_r} \quad (4a)$$

$$M_{pump} = \frac{V_D}{2\pi n_r} (p_{em} - p_{im}) \quad (4b)$$

$$M_{fr} = \frac{V_D}{2\pi n_r} (c_{fric,1} N_{ratio}^2 + c_{fric,2} N_{ratio} + c_{fric,3}) \quad (4c)$$

where V_D is the engine displacement, r_c the compression rate, q_{HV} the specific heating value of the fuel, and $N_{ratio} = \frac{N_{ice}}{1000}$ is the engine speed scaled.

Cylinder Outlet Temperature

The original model for cylinder out temperature requires the solution of a nonlinear set of equations in order to determine the residual gas fraction. Because of this a new model, found in [9], that assumes no residual gases was used. The equations are presented below, and a validation of cylinder out temperature in combination with exhaust manifold temperature is found in [Figure 2](#).

$$T_{eo} = \eta_{sc} \left(\frac{p_{em}}{p_{im}} \right)^{\frac{1}{\gamma_a}} r_c^{1-\gamma_a} \left(\frac{q_{in}}{c_{pa}} + T_{im} r_c^{\gamma_a-1} \right) \quad (5)$$

In [\(5\)](#) γ_a is the heat capacity ratio of air, T_{im} is the temperature in the intake manifold and η_{sc} is Seiliger cycle efficiency which compensates for non-ideal cycle behavior.

Exhaust Manifold Inlet Temperature

Due to the heat losses present in the exhaust manifold a temperature cooling model is added, between the cylinder outlet and the turbine inlet, to get a more reliable value on the temperature entering the turbine. Including the heat loss in the exhaust manifold, the temperature entering the turbine T_{em} is described as

$$T_{em} = T_{amb} + (T_{eo} - T_{amb})e^{\frac{-h_{tot}A_{pipe}}{c_{pe}(W_f + W_{ci})}} \quad (6)$$

where h_{tot} is the heat transfer coefficient between the exhaust pipe and the surrounding air, A_{pipe} is the pipe internal surface area, c_{pe} the heat capacity of the exhaust gases and T_{amb} is the ambient temperature surrounding the system. The model is found in [10]. The model validation can be found in Figure 2, where (5) is used to calculate T_{eo} in (6).

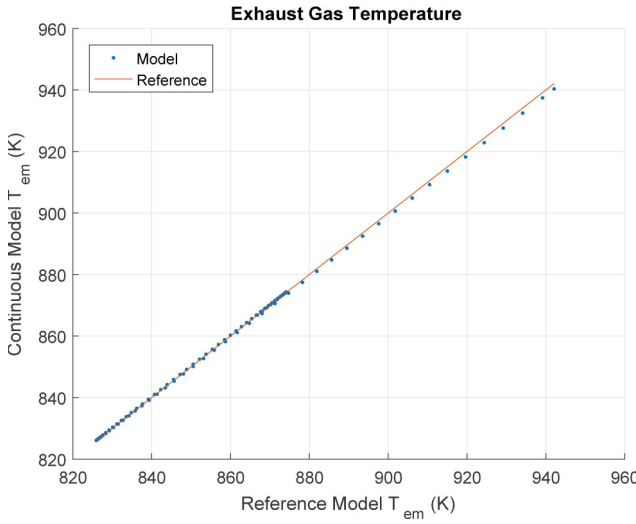


Figure 2. Cylinder out gas temperature model validation, comparison between the model and reference.

Compressor Power

The power delivered from the compressor P_c is described by equation (7e), which is dependent on the compressor efficiency η_c which is described in equation (7d). The following equations are used to calculate the compressor efficiency

$$\pi = (\Pi_c - 1)^{c_\pi} \quad (7a)$$

$$\chi = \begin{bmatrix} \pi_c - \pi_{c,opt} \\ W_c - W_{c,opt} \end{bmatrix} \quad (7b)$$

$$Q = \begin{bmatrix} q_1 & q_3 \\ q_3 & q_4 \end{bmatrix} \quad (7c)$$

$$\eta_c = \eta_{c,max} - \chi^T Q \chi \quad (7d)$$

$$P_c = \frac{W_c c_{pa} T_{cb} (\Pi_c^{\frac{\gamma-1}{\gamma}} - 1)}{\eta_c} \quad (7e)$$

where W_c is the mass flow of air flowing through the compressor, R_a is the gas constant of air, R_c is the radius of the compressor wheel, T_{cb} is the temperature before the compressor, and p_{amb} is the ambient pressure. The model is found in [2].

Compressor Mass Flow

Air mass flow delivered by the compressor is mainly dependent of the pressure ratio over the compressor and the compressor rotational speed. The model is found in [2]. The compressor mass flow is described by

$$W_c = \frac{p_{amb} \pi R_c^3 \omega_{tc} \phi_c}{R_a T_{amb}} \quad (8a)$$

$$\psi_c = \frac{2 c_{pa} T_{amb} (\Pi_c^{1-1/\gamma_a} - 1)}{R_c^2 \omega_{tc}^2} \quad (8b)$$

$$\Pi_c = \frac{p_{im}}{p_{amb}} \quad (8c)$$

$$c_{\psi 1}(\omega_{tc}) = c_{\omega \psi 1} \omega_{tc}^2 + c_{\omega \psi 2} \omega_{tc} + c_{\omega \psi 3} \quad (8d)$$

$$c_{\phi 1}(\omega_{tc}) = c_{\omega \phi 1} \omega_{tc}^2 + c_{\omega \phi 2} \omega_{tc} + c_{\omega \phi 3} \quad (8e)$$

$$\phi_c = \sqrt{\frac{1 - c_{\psi 1}(\Psi_c - c_{\psi 2})^2}{c_{\phi 1}}} + c_{\phi 2} \quad (8f)$$

where R_c is the compressor wheel radius and ω_{tc} is the rotational speed of the compressor.

Cylinder Air Flow

The mass flow into the cylinders is governed by

$$W_{ei} = \eta_{vol}(p_{im}, N_{ice}) \frac{p_{im} N_{ice} V_D}{60 n_r R_a T_{im}} \quad (9)$$

$$\eta_{vol}(p_{im}, \omega_{ice}) = c_{vol,1} \sqrt{p_{im}} + c_{vol,2} \sqrt{N_{ice}} + c_{vol,3} \quad (10)$$

The model is found in [2]. The division by 60 in (9) converts the engine speed N_{ice} from rpm to rps.

Cylinder Fuel Flow

The fuel flow into the cylinders is controlled using u_f . The relation between the control signal and mass flow of fuel W_f into the cylinders is

$$W_f = u_\delta N_{ice} n_{cyl} \frac{10^{-6}}{60n_r} \quad (II)$$

Variable Geometry Turbine

The turbine mass flow is described by

$$f_{VGT}(u_{VGT}) = c_{f2} + \dots \\ c_{f1} \sqrt{\max\left(0, 1 - \left(\frac{u_{VGT} - c_{VGT,2}}{c_{VGT,1}}\right)^2\right)} \quad (12a)$$

$$f_{VGT}(u_{VGT}) = c_{f2} + \dots \\ c_{f1} \sqrt{1 - \left(\frac{u_{VGT} - c_{VGT,2}}{c_{VGT,1}}\right)^2} \quad (12b)$$

$$W_t = \frac{A_{VGT,max} f_{VGT} p_{em} \sqrt{1 - \Pi_t^{K_t}}}{T_{em} R_e} \quad (12c)$$

The control signal to the VGT, u_{VGT} changes the effective area of the VGT opening. The model is the same as in [2], but the max-selector is removed (compare equation (12a) with (12b)), the selector is not kept, since it is not a continuous function. The equation (12b) is continuous over the interval of interest for the control signal u_{VGT} and the max-selector has no effect on the calculation for the valid range of u_{VGT} , this can be seen in Figure 3.

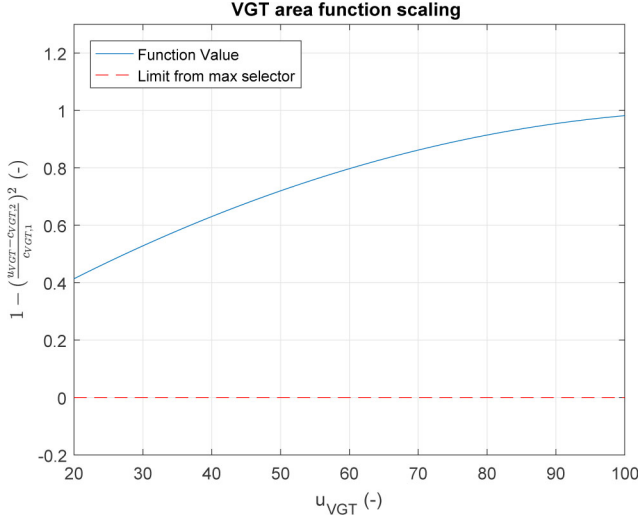


Figure 3. Function value inside the square root in (12a) as a function of the control signal u_{VGT} . The limit determined by the max selector in (12a) is clearly not affecting the function value.

Turbine Efficiency and Power

The original model for turbine efficiency in [2] is not continuously differentiable and was therefore replaced. The new model is found in [9]. Comparing the two models, the main difference is the choice of treating parameter c_m as a constant or as a function. The function used

to describe c_m in [2] is not continuously differentiable, therefore the model from [2] was chosen. The used model is found below. A validation is found in Figure 4 and 5.

$$BSR = \frac{R_t W_t}{\sqrt{2c_{pe} T_{em} \left(1 - \Pi_t^{\frac{\gamma_e - 1}{\gamma_e}}\right)}} \quad (13a)$$

$$\eta_{tm} = \eta_{tm,max} - c_m (BSR - BSR_{opt})^2 \quad (13b)$$

$$P_{t,tm} = \eta_{tm} W_t c_{pe} T_{em} \left(1 - \Pi_t^{\frac{\gamma_e - 1}{\gamma_e}}\right) \quad (13c)$$

In (13), Π_t is the pressure ratio over the turbine, R_t is the turbine wheel radius, c_m is a scaling constant, $\eta_{tm,max}$ is the maximum turbine efficiency, BSR_{opt} is the optimal BSR value.

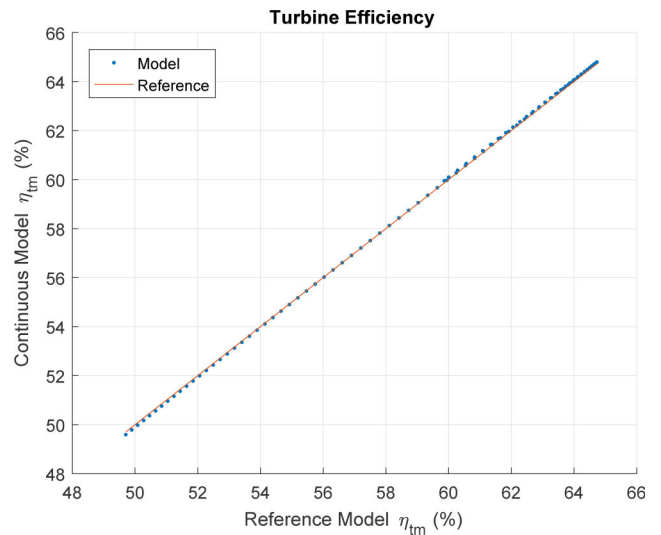


Figure 4. Turbine efficiency model validation, comparison between the model and reference.

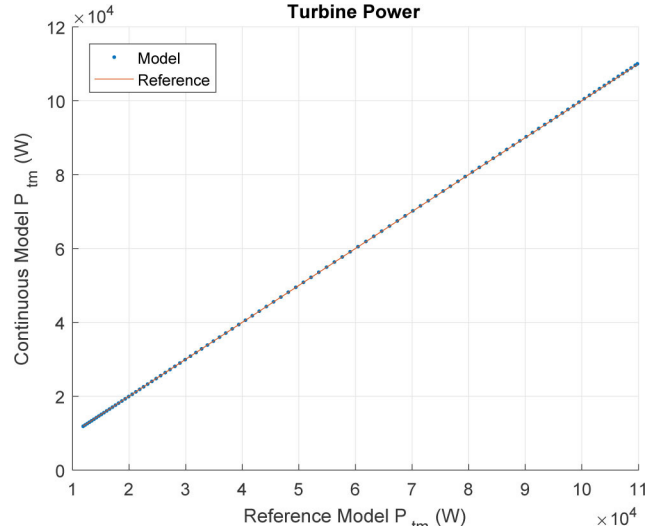


Figure 5. Turbine power model validation, comparison between the model and reference.

Intake Manifold

The pressure in the intake manifold is one of the states in the engine model. The change in intake manifold pressure is described by the mass balance

$$\frac{dp_{im}}{dt} = \frac{R_a T_{im}}{V_{im}} (W_c + W_{EGR} - W_{ei}) \quad (14)$$

Exhaust Manifold

The pressure in the exhaust manifold is one of the states in the engine model. The change in exhaust manifold pressure is described by the mass balance

$$\frac{dp_{em}}{dt} = \frac{R_e T_{em}}{V_{em}} (W_{ci} + W_f - W_t - W_{EGR}) \quad (15)$$

Turbocharger Shaft Speed

The turbocharger shaft speed is governed by the power balance between the power delivered from the turbine (P_{tm}) and the power consumed by the compressor (P_c).

$$\frac{d\omega_{tc}}{dt} = \frac{1}{J_{tc}\omega_{tc}} (P_{t,tm} - P_c) \quad (16)$$

Exhaust Gas Recirculation

The EGR system consists of two main components, a cooler and a valve. The cooler cools the hot exhaust gases before they are led into the intake manifold, the valve is used to control the mass flow of exhaust gas through the EGR system. The cooler is assumed to be ideal, which means that the recirculated exhaust gases enters the intake manifold with the same temperature as the inlet air. The original model, describing the effective area saturates at larger control signals, this behavior is hard to represent if the function is to be continuously differentiable. The function describing the effective area was therefore approximated by a continuously increasing function, the new model is plotted together with the original model in Figure 6. The new model was adapted from [4]. The EGR mass flow is given by the following equations

$$W_{EGR} = \frac{A_{eff,EGR} p_{em} \Psi(\Pi_{EGR})}{\sqrt{R_e T_{em}}} \quad (17a)$$

$$\Psi(\Pi_{EGR}) = \sqrt{\frac{2}{\Pi_{EGR}} \left(1 - \frac{1}{\Pi_{EGR}} \right)} \quad (17b)$$

$$A_{eff,EGR} = c_{EGR,1} u_{EGR} + c_{EGR,2} u_{EGR}^{c_{EGR,3}} \quad (17c) \quad (17d)$$

where $\Pi_{EGR} = \frac{p_{em}}{p_{im}}$. The fraction of burned gas in the intake manifold is F_{xim} , the oxygen fraction in the intake manifold X_{Oim} , exhaust manifold oxygen fraction X_{Oem} , and cylinder oxygen fraction X_{Oe} are described by

$$X_{Oe} = \frac{W_{ci} X_{Oim} - W_f (O/F)_s}{W_{ci} + W_f} \quad (18a)$$

$$\frac{dX_{Oim}}{dt} = \frac{R_a T_{im}}{p_{im} V_{im}} \left((X_{Oem} - X_{Oim}) W_{EGR} + (X_{Oc} - X_{Oim}) W_c \right) \quad (18b)$$

$$\frac{dX_{Oem}}{dt} = \frac{R_e T_{em}}{p_{em} V_{em}} (X_{Oe} - X_{Oem}) (W_f + W_{ei}) \quad (18c)$$

$$F_{xim} = 1 - \frac{X_{Oim}}{X_{Oc}}. \quad (18d)$$

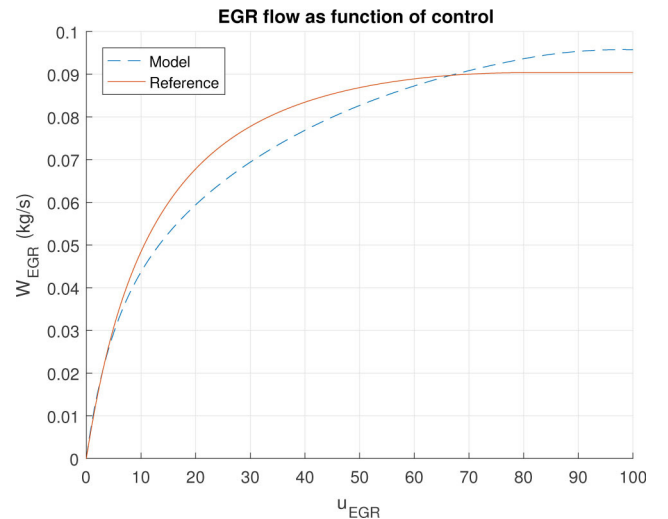


Figure 6. EGR mass flow model validation. The dashed blue line corresponds to the function implemented in the engine model describing the EGR mass flow and the solid red line is the reference EGR mass flow.

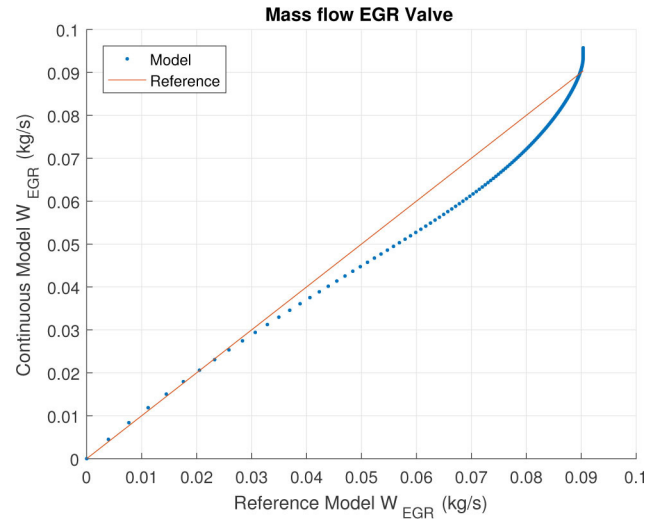


Figure 7. EGR mass flow model validation.

4. Optimal Control of a Heavy-Duty Diesel Engine Equipped with VGT And EGR

In this section the optimal control of the heavy duty diesel engine is presented. First the optimal steady-state behavior of the engine is presented, thereafter the optimal tip-ins are presented.

Optimal control of Diesel engines equipped with EGR is a difficult problem to solve because of the additional dynamic loop the EGR system introduces, which can easily cause the optimization to fail or exit prematurely, which was reported in [4].

Optimal Steady-State Load Points

The continuously differentiable model is used to find optimal steady-state operation by controlling the VGT and EGR actuators, while the engine speed and fuel injection is kept constant. If EGR control signal is increased from 0% to 100% open and VGT control signal is increased from 20% to 100% (20% corresponds to smallest possible VGT area), and this is made for the whole engine operation region (engine speed from 500 to 2000 rpm and fuel injection from 60 to 250 mg/cycle), it can be seen that the engine torque delivery is dependent on both VGT and EGR actuation (see for example Figure 9 or 10), where VGT and EGR are actuated for two different stationary operating conditions. There are at least two different methods for finding the optimal steady-state operation, either by brute force and sweeping VGT and EGR for each one of the different load points, or using optimization to find the optimal stationary selection of VGT and EGR for each load point. The optimization problem is formulated in equation (19), in which $\varphi = 1/\lambda$, and the goal is to maximize the delivered torque, given the fuel injection ($u_{\delta,0}$) and engine speed ($N_{e,0}$).

$$\begin{aligned} \max_u & M_{ice} \\ \text{s.t.} & f(x, u) = 0 \\ & u_\delta = u_{\delta,0} \\ & N_{ice} = N_{ice,0} \\ & F_{xim} \geq 20\% \\ & (1 - p_{im}/p_{em})u_{EGR} \geq 0 \\ & \Pi_c \leq \Pi_{c,surge} \\ & x_{min} \leq x \leq x_{max} \\ & u_{min} \leq u \leq u_{max} \\ & 0 \leq \phi \leq 1/\lambda_{min} \\ & N_{tc,min} \leq N_{tc} \leq N_{tc,max} \\ & BSR_{min} \leq BSR \leq BSR_{max} \end{aligned} \quad (19)$$

Figure 8 shows the torque delivered in each operating point where the fuel injection and engine speed is kept constant running the original MVEM model from [2], the EGR is kept at 0% and the VGT is adjusted from 20% to 100% (full VGT operation region, 20% is the

smallest possible VGT area setting). It is displayed in Figure 8 that for some operation points it is more efficient, in terms of torque delivery, when the VGT is not fully open. The green lines in the top left corner of the map in Figure 8 are restricted, due to the smoke limiter. The optimal VGT actuation at those engine loads is to open the VGT until the air to fuel limit is reached. When investigating steady-state operation and both EGR and VGT is taken into account it is visual that the delivered torque dependent on both actuators. Comparing Figures 9 and 10 shows the difference in the optimal VGT and EGR control for two different set points. It is visual that it is not always optimal with a fully open VGT.

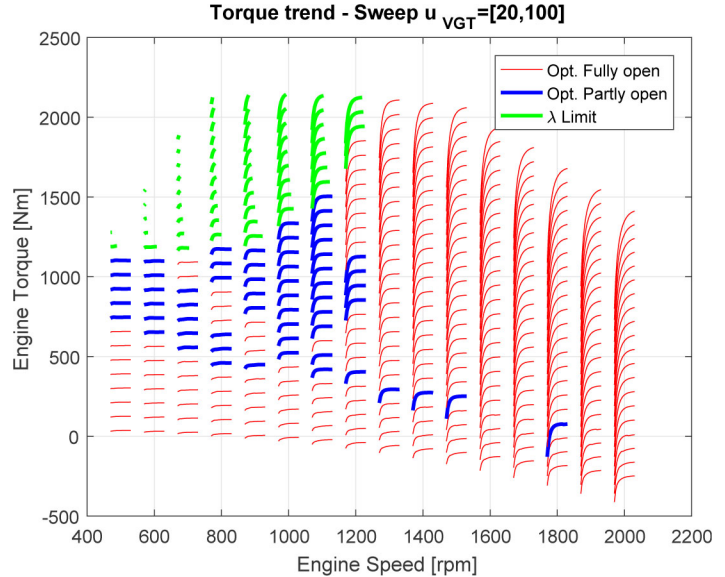


Figure 8. Engine map with VGT sweep overlay. In each sweep (red, blue or green line), the amount of injected fuel is constant, the engine speed is constant, $u_{EGR} = 0$ and $u_{VGT} = [20, 100]$. The green sweep lines are restricted by the engine air to fuel ratio. The y-value of each line represents the torque delivered by the engine model in each one of the load points, and the x-value of each line represents u_{VGT} from 20% to 100% (the center x-value of each line is located at the stationary engine speed).

Optimal Tip-in Maneuvers

The tip-ins are ran at a predetermined constant engine speed $N_{ice,0}$. At the start of the tip-in, the conditions are stationary, and the engine is delivering a certain predetermined brake torque $M_{ice,0}$. At the initial point, $t = 0$, the state is x_0 and the applied control signal is u_0 . At the final point, $t = t_f$, the conditions are again stationary, but the new state is x_f , the controls signal is u_f , and the engine is delivering the brake torque $M_{ice,f}$ that was requested from the tip-in. The initial and terminal conditions have been optimized to deliver the requested torque using minimum fuel, while keeping the EGR fraction in the intake manifold, F_{xim} , at, or above, 20 %. The motivation for these EGR levels was discussions with engineers working in the automotive industry. The optimal control problem objective is to perform the tip-in as fast as possible. The optimal control problem is formulated in equation (20).

The constraint $(1 - p_{im}(t)/p_{em}(t))u_{EGR}(t) \geq 0$ was found to be an effective way of forcing the EGR-massflow W_{EGR} to only go in the direction from the intake manifold, to the exhaust manifold. The first part, $(1 - p_{im}(t)/p_{em}(t))$ gives the sign of the flow direction, which must always be positive if EGR-massflow is desired. The

multiplication with $u_{EGR}(t)$ makes it possible to have a higher intake manifold pressure than exhaust manifold pressure if the EGR-valve is closed.

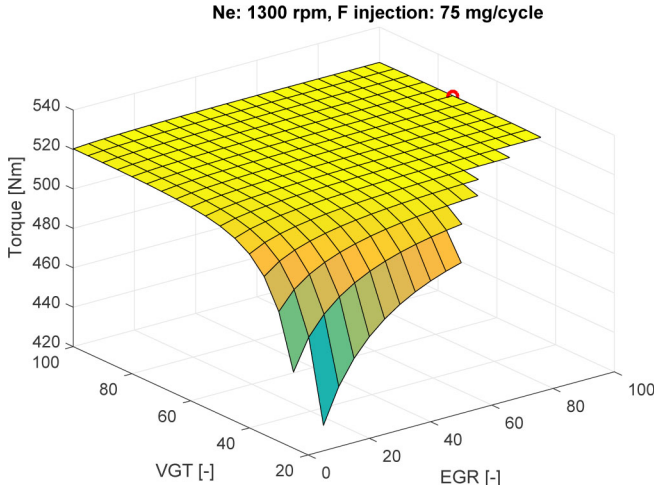


Figure 9. Stationary map, low load point, VGT and EGR actuators are controlled from minimum to maximum values, fuel injection and engine speed are kept constant.

$$\begin{aligned} \min_{u(t)} & t_f \\ \text{s.t.} & \end{aligned}$$

$$\begin{aligned} f(x(t), u(t)) &= 0 \\ x(0) &= x_0 \\ u(0) &= u_0 \\ x(t_f) &= x_f \\ u(t_f) &= u_f \\ \frac{du_{VGT}}{dt} &\leq dVGT_{max} \\ \frac{du_{VGT}}{dt} &\geq dVGT_{min} \\ \frac{du_{EGR}}{dt} &\leq dEGR_{max} \\ \frac{du_{EGR}}{dt} &\geq dEGR_{min} \\ M_{ice}(0) &= M_{ice,0} \\ M_{ice}(t_f) &= M_{ice,f} \\ N_{ice}(t) &= N_{ice,0} \\ F_{xim}(t) &\geq F_{xim,min} \\ (1 - p_{im}(t)/p_{em}(t))u_{EGR}(t) &\geq 0 \\ \Pi_c(t) &\leq \Pi_{c,surge} \\ x_{min} &\leq x(t) \leq x_{max} \\ u_{min} &\leq u(t) \leq u_{max} \\ 0 &\leq \phi(t) \leq 1/\lambda_{min} \\ N_{tc,min} &\leq N_{tc}(t) \leq N_{tc,max} \\ BSR_{min} &\leq BSR(t) \leq BSR_{max} \end{aligned} \tag{20}$$

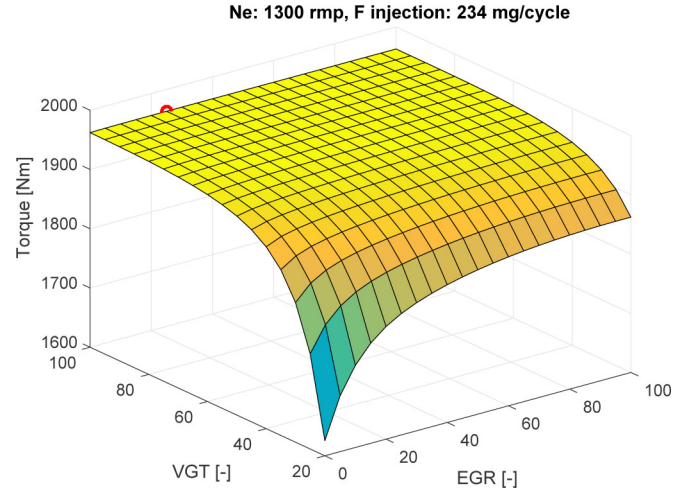


Figure 10. Stationary map, high load point, VGT and EGR actuators are controlled from minimum to maximum values, fuel injection and engine speed are kept constant.

Numerical Solution of the Optimal Control Problems

The numerical solution to the optimal control problems was obtained by discretizing the optimal control problems using local direct collocation (see [11] for an explanation) with four Legendre collocation points, and parameterizing the control signal as piecewise constant. The direct collocation algorithm was implemented using CasADi [12], and the resulting nonlinear program was solved using IPOPT [13].

5. RESULTS

This section presents the results. First the trade-off between tip-in duration and EGR fraction in the intake manifold is illustrated, then the optimal tip-in trajectory for the conditions that allow for the fastest possible tip-in is presented and discussed, thereafter a comparison of the optimal trajectory under increasing EGR recirculation demand is presented and discussed.

When solving the optimal tip-in problem (20) a trade-off between tip-in duration and minimum amount of exhaust gas in the intake manifold needs to be made. Figure 11 illustrates the trade-off. From the figure the exponential increase in tip-in duration with increasing EGR demand is clearly illustrated.

The fastest possible tip-in is achieved when there is no demand on the amount of EGR gas in the intake manifold. The result from such a tip-in is illustrated in Figures 12 through 15. The active constraint during the tip-in is the smoke limiter. See figure 12 in which λ is at the minimum level during the major part of the tip-in. It leaves minimum λ at the end of the tip-in, which is due to two things. The first is the problem formulation, and the second is that the system is stationary at the terminal boundary. To achieve stationarity in the fastest possible way the optimization finds a flapping actuation of the controls which results in the system leaving minimum λ for a short while, see Figure 12 at time 4 seconds.

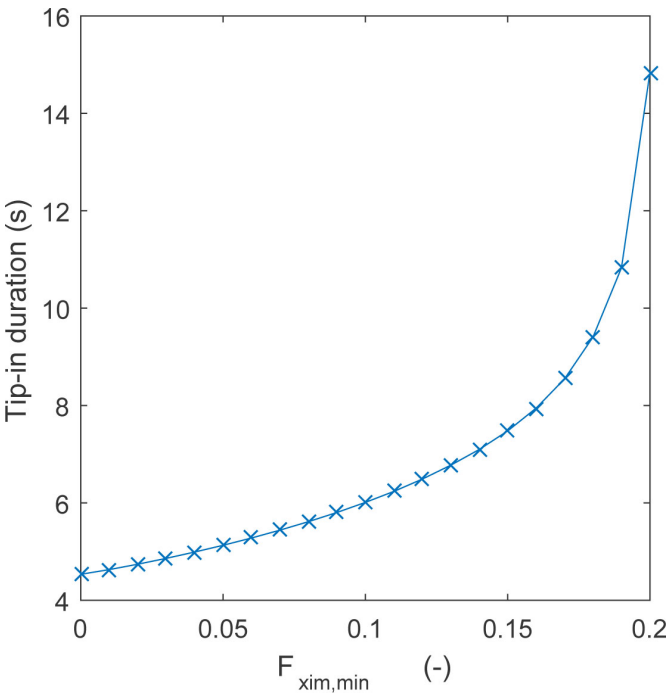


Figure 11. Trade-off between tip-in duration and minimum amount of EGR in the intake manifold. Feasible region to the left of the line.

The dominating dynamics during the tip-in is the turbocharger. This was concluded by performing a sensitivity analysis of the turbocharger inertia. The results showed that the solution characteristics were exactly the same but the tip-in duration was either slower or faster depending if there was an increase or decrease in inertia. The turbocharger inertia limits how fast the turbocharger can accelerate, which limits the compressor air mass flow, which limits how much fuel that can be injected, which finally limits the torque.

During the tip-in, EGR and VGT are actuated in such a way that the turbocharger reaches the critical speed, where it delivers the necessary mass flow, as fast as possible. Notice Figure 14, in which it is seen that the compressor is working at points far to the right, delivering a high air mass flow. The EGR valve is closed at the beginning of the tip-in and thereby reducing the burned gas fraction in the intake manifold. This results in higher exhaust gas temperatures leaving the cylinder, which in turn results in a higher temperature in the exhaust manifold, see Figure 13. The EGR valve is closed at a rate corresponding to the fastest possible actuation of the valve. The VGT is actuated such that a high power is delivered from the turbine, see Figure 15. The VGT is actuated at its fastest rate at the end of the interval, in order to reach stationary conditions as fast as possible.

When demanding a burned gas fraction in the intake manifold higher than zero, this limits how fast the tip-in can be performed. Three different cases of EGR constraints (three different values of $F_{xim,min}$ in (20)) are compared in Figures 16 and 17. The lines drawn in blue show the case when the minimum EGR-level in the intake manifold is zero, the red line show the case when the EGR-level is at or above 14 %, and the yellow line show the case when the EGR-level is at or above 20 %. The limiting constraint for all three cases is the smoke limiter. The major reason that the tip-ins are slower when EGR is increased is that there is less energy in the exhaust gas. This is seen in

Figure 17, where the lowered exhaust gas temperature due to EGR is illustrated. This results in a slower build up of turbocharger speed, seen in Figure 16. Notice in the same figure that the turbine and compressor efficiencies are moving on similar lines in all cases, and that the BSR is moving at the same line for all three cases. By studying both Figure 16 and 17 it can be seen that the characteristics are similar for all three cases.

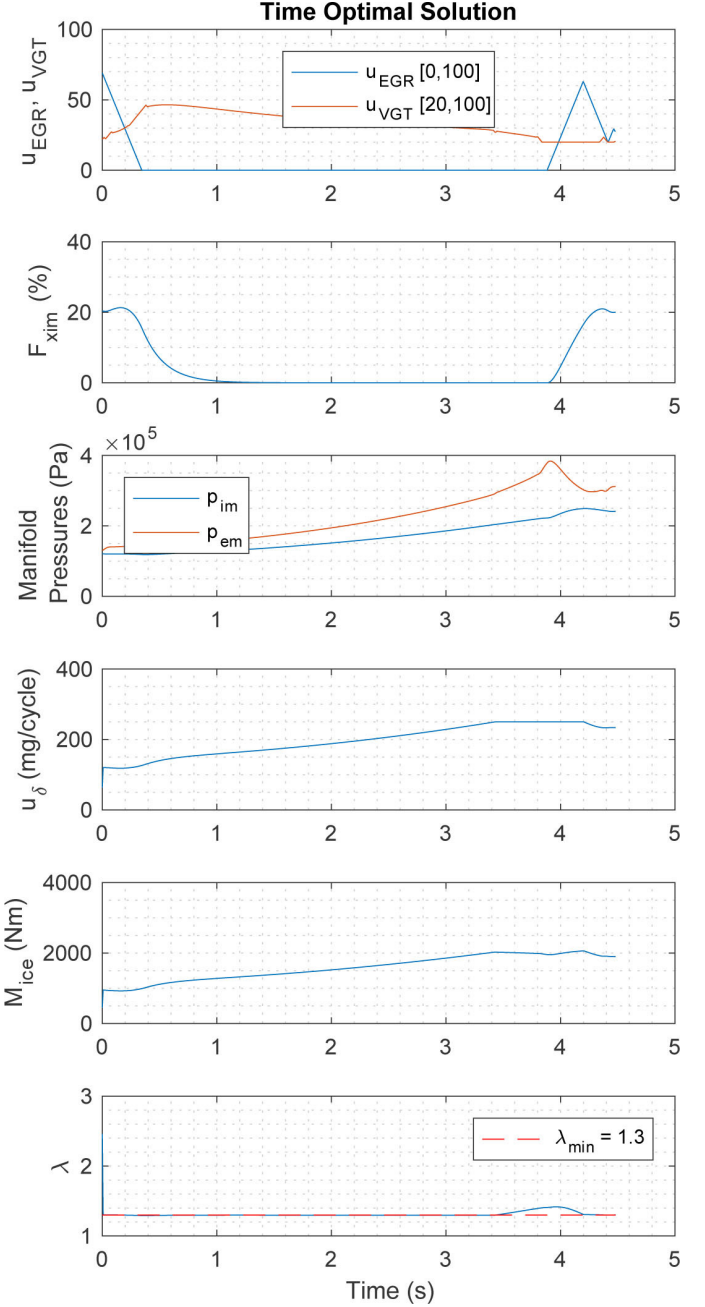


Figure 12. The optimal solution is to close the EGR as fast as possible, to control the transferred power from the turbine with the VGT. There is an increase in lambda at around 4 seconds, which occurs due to the extra fuel injected, to force the system into a stationary condition at the end time. The results have been subjected to a sensitivity analysis, testing the initial and terminal conditions, control actuation speed, turbocharger inertia, and the discretization method (direct multiple shooting was also used. See [14] for a description). The solution was proven stable for all mentioned cases.

6. CONCLUSION

A continuously differentiable model has been developed, based on a validated MVEM model, where all not continuously differentiable sub-models were changed. The errors induced by the transformation to a continuously differentiable were small, but it enables efficient computations with numerical optimal control solvers. With the use of optimal control, a minimum time tip-in problem has been solved, the results reveal non trivial solutions with respect to VGT and EGR actuation. The following conclusions were drawn:

- Optimal control can be used to find fuel optimal stationary load points.
- EGR fraction constraints ($F_{xim,min}$), effects the optimal tip-in time in an exponential way.
- The continuously differentiable model can be used to investigate both stationary and transient control.
- The dominating dynamics for the tip-ins is the turbocharger.
- The active constraint for the tip-ins is the smoke limiter.

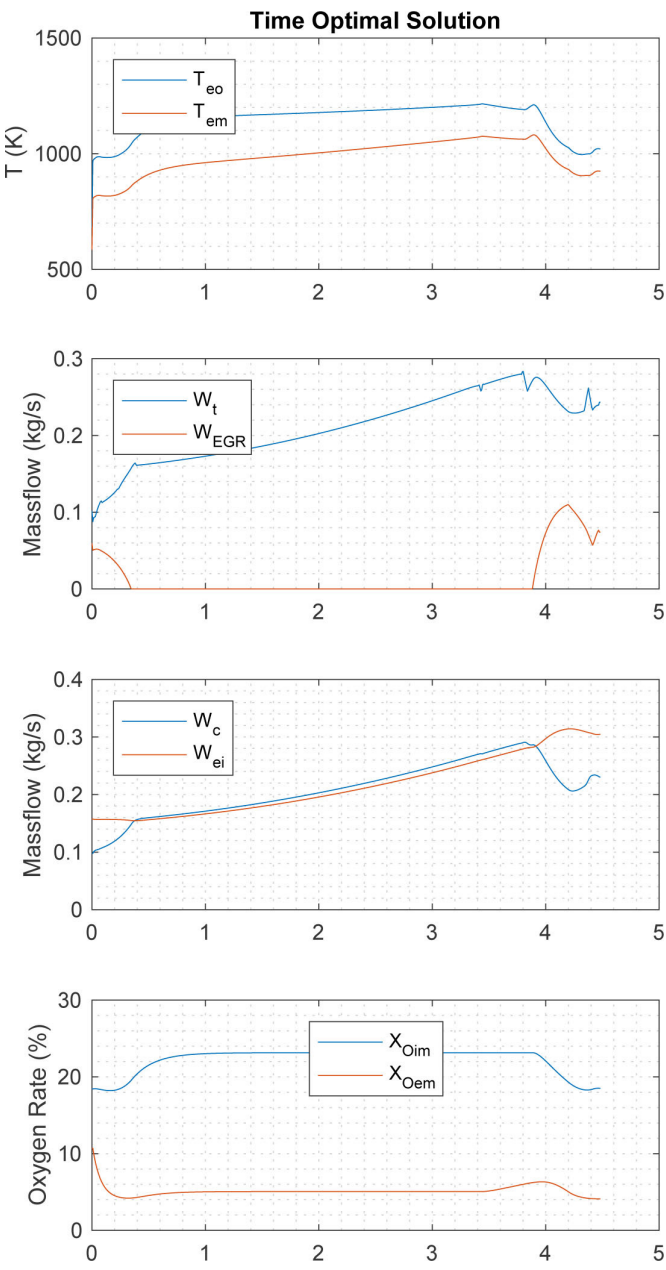


Figure 13. As a consequence of the EGR valve closing, the EGR mass flow decreases, and the turbine mass flow increases, to make more power available at the compressor.

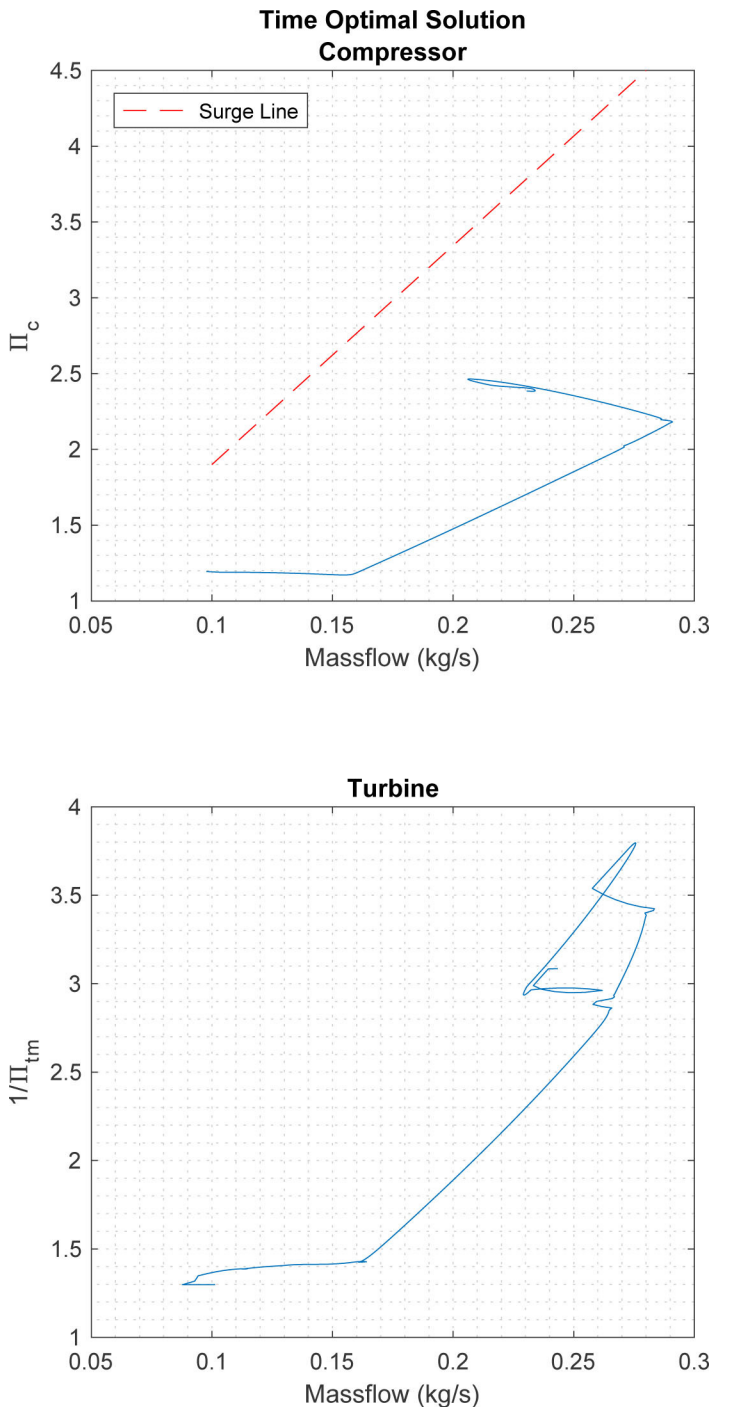


Figure 14. The working points in the compressor and turbine maps. The transient in the compressor map starts at a low mass flow (0.1 kg/s) and ends at a higher mass flow (0.2 kg/s). The movement is made where the highest possible mass flow is available, for the current pressure ratio. The turbine has the same behavior, the expansion ratio increases while the mass flow increases.

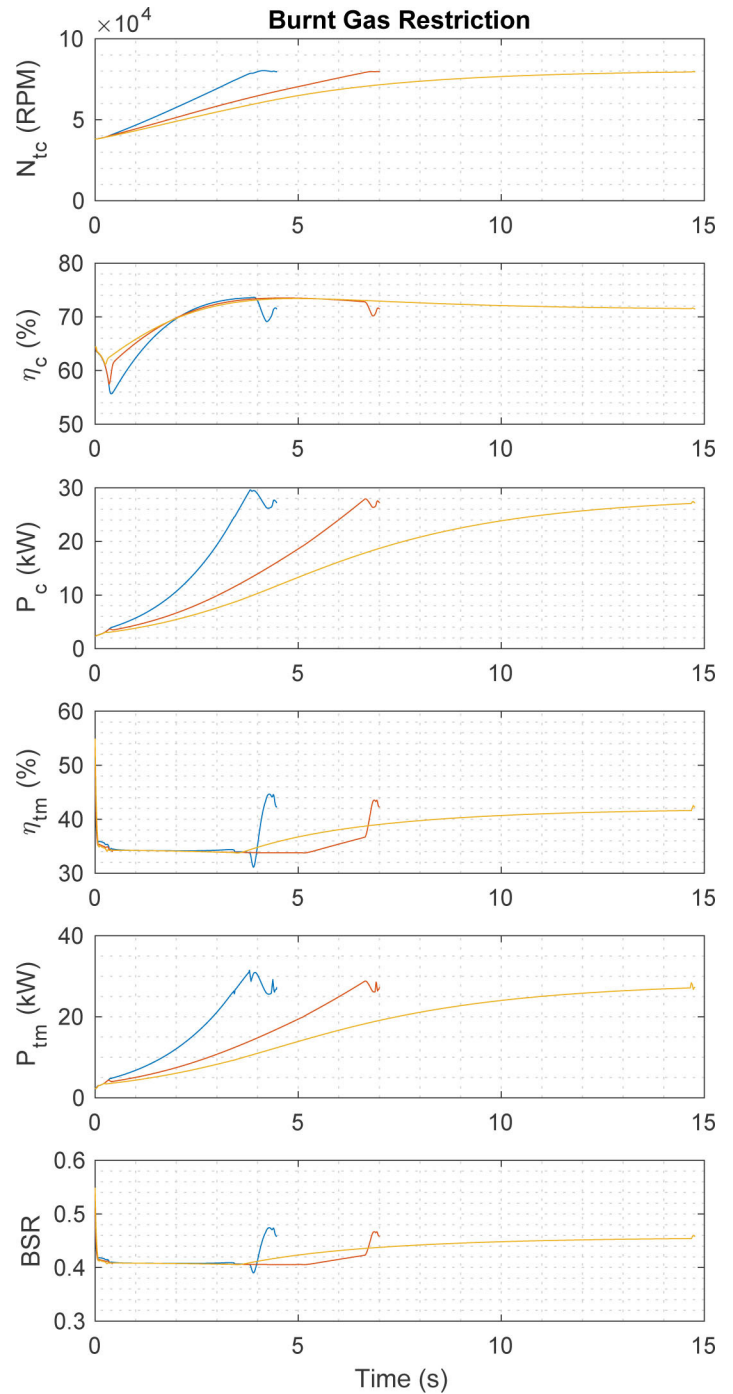
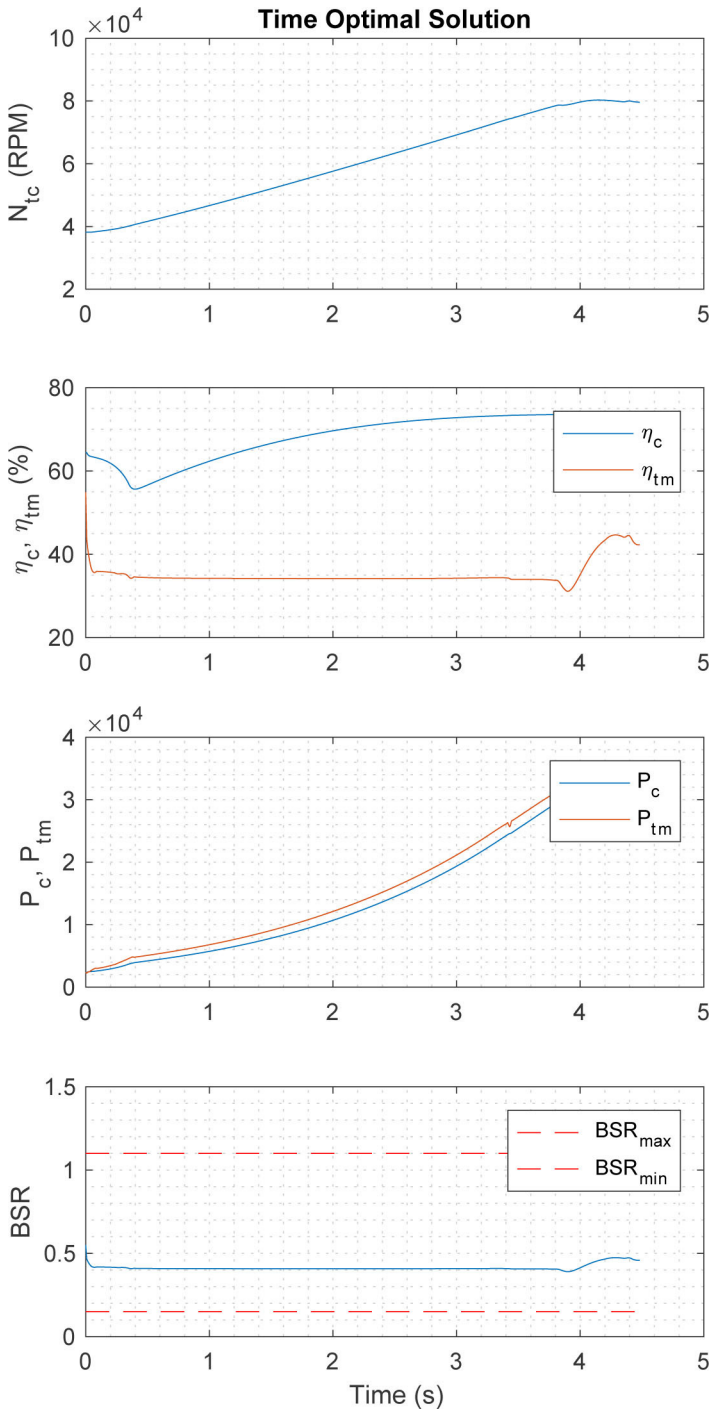


Figure 15. The turbine power is higher than the compressor power due to the friction inside the turbocharger. The BSR is clearly not restricted by any limitations..

Figure 16. Three different solutions where the minimum requirement of burned gas in the intake manifold ($F_{xim} \geq 0, 15, 20\%$) has been taken into account, the main optimization goal is to minimize the time of the step-in. When there is no requirement on burned gas ($F_{xim} = 0$), the shortest solution is valid, and when the requirement is no less than 20% ($F_{xim} \geq 20\%$) the most time consuming solutions is valid.

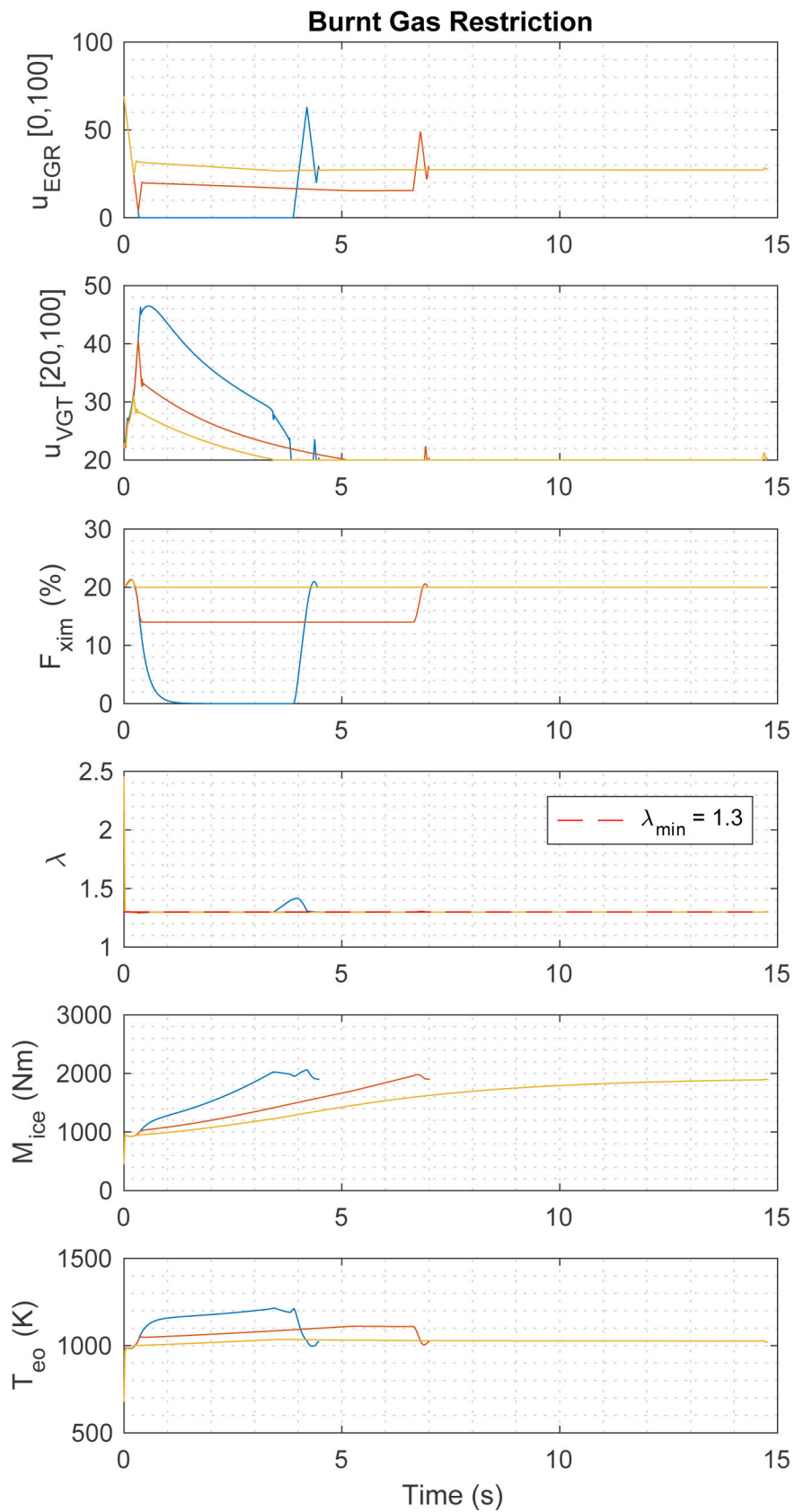


Figure 17. It is visual that the maximum amount of power from the turbine and the compressor are very different for the three different solutions. The least time consuming solution clearly has the highest turbine power and the least fuel consuming solution has the lowest power demand.

Table 1. Symbol description

Symbol	Description	Unit
u_f	Injected fuel	mg/cycle
u_{EGR}	EGR actuator	-
u_{VGT}	VGT actuator	-
W	Mass flow	kg/s
p	Pressure	Pa
T	Temperature	K
BSR	Blade speed ratio	-
J	Inertia	$\text{kg} \cdot \text{m}^2$
M	Torque	Nm
P	Power	W
t_f	End time	s
λ	Air-fuel equivalence ratio	-
ρ	Density	kg/m^3
ω	Rotational speed	rad/s
X	Oxygen fraction	-
η	Efficiency	-
n_{cyl}	Number of cylinders	-
V_D	Cylinder Volume	m^3
Π	Pressure ratio	-

Table 2. Index description

Index	Description
a	air
c	compressor
t	turbine
tm	turbine mechanical
tc	turbocharger
$c, surge$	compressor surge limit
em	exhaust manifold
f	fuel
ei	Engine in
gen	generator electrical
ice	Internal combustion engine
im	Intake manifold
max	maximum
min	minimum

References

1. Eriksson Lars and Nielsen Lars. *Modeling and control of engines and drivelines*. John Wiley and Sons Ltd, 2014.
2. Wahlström Johan and Eriksson Lars. Modelling diesel engines with a variable geometry turbocharger and exhaust gas recirculation by optimization of model parameters for capturing non-linear system dynamics. *Proceedings of the Institution of Mechanical Engineers, Part D, journal of automobile engineering*, 225(7):960–986, 2011.
3. Diehl Moritz, Bock Hans Georg, Diedam Holger, and Wieber Pierre-Brice. Fast direct multiple shooting algorithms for optimal robot control. In *Fast Motions in Biomechanics and Robotics*, Heidelberg, Germany, 2005.
4. Asprion Jonas. *Optimal Control of Diesel Engines: Modeling, Numerical Methods and Applications*. PhD thesis, ETH Zürich, Sonneggstrasse 3, CH-8092 Zurich, Switzerland, 2013.
5. Stefanopoulou A. G., Kolmanovsky I., and Freudenberg J. S.. Control of variable geometry turbocharged diesel engines for reduced emissions. *IEEE Transactions on Control Systems Technology*, 8(4):733–745, Jul 2000. ISSN 1063-6536. doi:[10.1109/87.852917](https://doi.org/10.1109/87.852917).
6. Flärdh, O. Ericsson, G. Klingborg E., and Mårtensson J.. Optimal air path control during load transients on a spark ignited engine with variable geometry turbine and variable valve timing. *IEEE Transactions on Control Systems Technology*, 22(1):83–93, Jan 2014. ISSN 1063-6536.
7. Nezhadali Vaheed. Modeling and Optimal Control of Heavy-duty Powertrains. PhD thesis, Linköping University, Sweden, 2016.
8. Guzzella L. and Amstutz A.. Control of diesel engines. *IEEE Control Systems*, 18(5):53–71, Oct 1998. ISSN 1066-033X. doi:[10.1109/37.722253](https://doi.org/10.1109/37.722253).
9. Sivertsson Martin and Eriksson Lars. Modeling for Optimal Control: A Validated Diesel-Electric Powertrain Model. *SIMS 2014 - 55th International Conference on Simulation and Modelling*, Ålborg, Denmark, 2011.
10. Eriksson, L., "Mean Value Models for Exhaust System Temperatures," SAE Technical Paper [2002-01-0374](https://doi.org/10.4271/2002-01-0374), 2002, doi:[10.4271/2002-01-0374](https://doi.org/10.4271/2002-01-0374).
11. Biegler Lorenz T.. *Nonlinear Programming: Concepts, Algorithms, and Applications to Chemical Processes*. MOS-SIAM Series on Optimization, 2010.
12. Andersson Joel. A General-Purpose Software Framework for Dynamic Optimization. PhD thesis, Arenberg Doctoral School, KU Leuven, Department of Electrical Engineering (ESAT/SCD) and Optimization in Engineering Center, Kasteelpark Arenberg 10, 3001-Heverlee, Belgium, October 2013.
13. Wächter, Andreas and Biegler, Lorenz T. On the implementation of a primal-dual interior point filter line search algorithm for large-scale nonlinear programming, 2006.
14. Betts John T.. *Practical Methods for Optimal Control and Estimation Using Nonlinear Programming*. SIAM, second edition, 2010.

CONTACT INFORMATION

viktor.leek@liu.se

kristoffer.ekberg@liu.se

Acknowledgments

FUNDING ACKNOWLEDGMENT

This work was supported by the Vinnova Industry Excellence Center: LINK-SIC Linköping Center for Sensor Informatics and Control, the Swedish Energy Agency, and Scania CV AB.

The Engineering Meetings Board has approved this paper for publication. It has successfully completed SAE's peer review process under the supervision of the session organizer. The process requires a minimum of three (3) reviews by industry experts.

All rights reserved. No part of this publication may be reproduced, stored in a retrieval system, or transmitted, in any form or by any means, electronic, mechanical, photocopying, recording, or otherwise, without the prior written permission of SAE International.

Positions and opinions advanced in this paper are those of the author(s) and not necessarily those of SAE International. The author is solely responsible for the content of the paper.

ISSN 0148-7191

<http://papers.sae.org/2017-01-0611>